Science Advances
AAAS

advances.sciencemag.org/cgi/content/full/7/2/eabc2962/DC1

Supplementary Materials for

Heating events in the nascent solar system recorded by rare earth element isotopic fractionation in refractory inclusions

J. Y. Hu*, N. Dauphas, F. L. H. Tissot, R. Yokochi, T. J. Ireland, Z. Zhang, A. M. Davis, F. J. Ciesla, L. Grossman, B. L. A. Charlier, M. Roskosz, E. E. Alp, M. Y. Hu, J. Zhao

*Corresponding author. Email: jingya@uchicago.edu

Published 6 January 2021, *Sci. Adv.* **7**, eabc2962 (2021)
DOI: 10.1126/sciadv.abc2962

This PDF file includes:

Supplementary Online Materials

Modeling of Stable Isotopic Fractionation Induced by Evaporation and Condensation

1. Speciation of REEs during Evaporation and Condensation

In this section, we calculate the vapor pressures of the different species of a REE in equilibrium with hibonite. Hibonite is a highly refractory mineral that has been implicated in establishing the REE abundance pattern of group II CAIs (*15, 19*). According to equilibrium thermodynamics (*15, 19*), REEs can exist in the form of 6 species under solar nebula conditions, where 3 species are present in gaseous forms (noted as $M^0{}_{(g)}$, $M^{2+}O_{(g)}$, $M^{4+}O_{2(g)}$) and the other 3 species substitute for Ca in solid solution in refractory minerals such as hibonite and perovskite ($M^{2+}O_{(s)}$, $M^{3+}O_{1.5(s)}$, $M^{4+}O_{2(s)}$). At equilibrium, the partial pressures and molar densities of different species are related to each other through the following equilibria:

$$M_{(g)} + O_{(g)} = MO_{(g)},$$

$$K_1 = \frac{P_{MO}}{P_M P_O}, \tag{S1}$$

$$2MO_{1.5(s)} = 2M_{(g)} + 3O_{(g)},$$

$$K_2 = \frac{{P_M}^2 {P_O}^3}{\left(\chi_{MO_{1.5}} n_{MO_{1.5}}/n_{Ca}\right)^2}, \tag{S2}$$

$$M_{(g)} + 2O_{(g)} = MO_{2(g)},$$

$$K_3 = \frac{P_{MO_2}}{P_M {P_O}^2}, \tag{S3}$$

$$MO_{2(s)} = M_{(g)} + 2O_{(g)},$$

$$K_4 = \frac{P_M {P_O}^2}{\chi_{MO_2} n_{MO_2}/n_{Ca}}, \tag{S4}$$

$$MO_{(s)} = M_{(g)} + O_{(g)},$$

$$K_5 = \frac{P_M P_O}{\chi_{MO} n_{MO}/n_{Ca}}, \tag{S5}$$

where K_1–K_5 are the equilibrium constants of the chemical reactions, P_ℓ, χ_ℓ, and n_ℓ, are, respectively, the partial pressures, activity coefficients, and solid molar densities of the REE considered (number of moles of M, MO, MO_2), P_O is the partial pressure of atomic oxygen (the value of P_O for solar nebula conditions is provided in (*3, 15*)), and n_{Ca} is the solid molar

density of Ca (condensed REEs are expected to substitute for Ca in refractory minerals). One can rearrange the equations above and write P_M, P_{MO}, P_{MO_2}, n_{MO_2}, n_{MO} as functions of P_O, K_1 to K_5, χ_M, χ_{MO}, χ_{MO_2}, $n_{MO_{1.5}}$ and n_{Ca},

$$P_M = \sqrt{K_2}\,\frac{1}{{P_O}^{1.5}}\frac{\chi_{MO_{1.5}}}{n_{Ca}}n_{MO_{1.5}}, \tag{S6}$$

$$P_{MO} = K_1\sqrt{K_2}\,\frac{1}{\sqrt{P_O}}\frac{\chi_{MO_{1.5}}}{n_{Ca}}n_{MO_{1.5}}, \tag{S7}$$

$$P_{MO_2} = \sqrt{K_2}K_3\sqrt{P_O}\,\frac{\chi_{MO_{1.5}}}{n_{Ca}}n_{MO_{1.5}}, \tag{S8}$$

$$n_{MO_2} = \frac{\sqrt{K_2}}{K_4}\sqrt{P_O}\,\frac{\chi_{MO_{1.5}}}{\chi_{MO_2}}n_{MO_{1.5}}, \tag{S9}$$

$$n_{MO} = \frac{\sqrt{K_2}}{K_5}\frac{1}{\sqrt{P_O}}\frac{\chi_{MO_{1.5}}}{\chi_{MO}}n_{MO_{1.5}}. \tag{S10}$$

The total molar density of a given condensed REE is given by the sum of 3 solid species,

$$n_{Mtot} = n_{MO} + n_{MO_{1.5}} + n_{MO_2}. \tag{S11}$$

Accordingly, one can write $n_{MO_{1.5}}$ as a function of n_{Mtot} using Eqs. S9–S11,

$$n_{MO_{1.5}} = \frac{n_{Mtot}}{1+\frac{\sqrt{K_2}}{K_5}\frac{1}{\sqrt{P_O}}\frac{\chi_{MO_{1.5}}}{\chi_{MO}}+\frac{\sqrt{K_2}}{K_4}\sqrt{P_O}\frac{\chi_{MO_{1.5}}}{\chi_{MO_2}}}. \tag{S12}$$

In the same manner, the partial pressures of $M_{(g)}$, $MO_{(g)}$ and $MO_{2\,(g)}$ can be written as a function of n_{Mtot} and P_{Mtot},

$$P_M = \frac{1}{P_O}\frac{1}{\frac{1}{K_5\chi_{MO}}+\frac{\sqrt{P_O}}{\sqrt{K_2}\chi_{MO_{1.5}}}+\frac{P_O}{K_4\chi_{MO_2}}}\frac{n_{Mtot}}{n_{Ca}}, \tag{S13}$$

$$P_{MO} = K_1\frac{1}{\frac{1}{K_5\chi_{MO}}+\frac{\sqrt{P_O}}{\sqrt{K_2}\chi_{MO_{1.5}}}+\frac{P_O}{K_4\chi_{MO_2}}}\frac{n_{Mtot}}{n_{Ca}}, \tag{S14}$$

$$P_{MO_2} = K_3P_O\frac{1}{\frac{1}{K_5\chi_{MO}}+\frac{\sqrt{P_O}}{\sqrt{K_2}\chi_{MO_{1.5}}}+\frac{P_O}{K_4\chi_{MO_2}}}\frac{n_{Mtot}}{n_{Ca}}, \tag{S15}$$

$$P_M = \frac{1/P_O}{1/P_O+K_1+K_3P_O}P_{Mtot} = x_MP_{Mtot}, \tag{S16}$$

$$P_{MO} = \frac{K_1}{1/P_O+K_1+K_3P_O}P_{Mtot} = x_{MO}P_{Mtot}, \tag{S17}$$

$$P_{MO_2} = \frac{K_3P_O}{1/P_O+K_1+K_3P_O}P_{Mtot} = x_{MO_2}P_{Mtot}. \tag{S18}$$

where x_ℓ are the mole fraction of the various gas species. We also have for the total vapor pressure of a REE,

$$P_{Mtot} = \frac{1/P_O + K_1 + K_3 P_O}{\frac{1}{K_5 \chi_{MO}} + \frac{\sqrt{P_O}}{\sqrt{K_2}\chi_{MO_{1.5}}} + \frac{P_O}{K_4 \chi_{MO_2}}} \frac{n_{Mtot}}{n_{Ca}} = \kappa \frac{n_{Mtot}}{n_{Ca}}, \quad \text{(S19)}$$

where κ is a factor that relates the equilibrium vapor pressure to the concentration (molar density) in the solid. Equations S13–S15 can be used to calculate the equilibrium pressures of gaseous species if the molar density of the REEs in solid, temperature, thermodynamic constants, and oxygen partial pressure are known.

2. REE Abundance and Stable Isotopic Fractionation during Evaporation

In this section, our goal is to develop a quantitative model of the depletions and stable isotopic fractionations of all REEs during evaporation. Most REEs are thought to have been quantitative evaporated during the first stage of evaporation envisioned here. The only REEs that were not quantitatively evaporated are the most refractory ones, notably Gd and Dy. In fine-grained CAIs, we find that these REEs are highly depleted relative to moderately refractory REEs and have light isotopic compositions. This is more readily explained if the signature of group II REE patterns in CAIs were inherited from an episode of evaporation, whereby the most refractory REEs were only partially evaporated in an undersaturated medium, resulting in their light isotope enrichment in the gas phase, which latter partially re-condensed to form CAIs with group II REE patterns. For this first evaporation stage, we are therefore primarily interested in the isotopic composition of the vapor. Our primary aim here is to use the isotopic composition of the most refractory REEs to put constraints on the rate of heating and duration of the evaporation episode. According to the Hertz-Knudsen equation, the net flux for each REE i during evaporation is given by,

$$J_i = \sum_\ell \frac{\gamma_{\ell,i}\left(P_{eq,\ell,i} - P_{\ell,i}\right)}{\sqrt{2\pi m_{\ell,i} RT}}, \quad \text{(S20)}$$

where ℓ enumerates the gaseous species $M_{(g)}$, $MO_{(g)}$ and $MO_{2_{(g)}}$, $\gamma_{\ell,i}$ and $m_{\ell,i}$ are the condensation/evaporation coefficients and masses of the corresponding species, R is the gas constant, $P_{\ell,i}$ and $P_{eq,\ell,i}$ are the partial and equilibrium vapor pressures, respectively. The equilibrium vapor pressure $P_{eq,\ell,i}$ in Eq. S20 is the partial pressure that is in equilibrium with the condensate at temperature T, as is derived in Eqs. S13–S15.

We consider a model where refractory inclusions of similar sizes and evenly distributed in space are evaporated. This model is similar to those applied to closed-system condensation/evaporation and chondrule formation (*22-24, 26, 27*). Under these conditions, we do not need to track a whole ensemble of refractory inclusions and can only consider a single CAI of radius r surrounded by a parcel of gas of finite volume $V_g = 4\pi\mathcal{R}^3/3$ with no-flux boundary conditions at the boundaries ($\mathcal{R}$ is the radius of the system inclusion+gas, which is much larger than the radius r of the inclusion itself). From a practical point of view, this is equivalent to considering a local closed-system. We assume that the driver for evaporation is heating, with the temperature increasing linearly with time, $T(t) = T_0 + \Phi t$, where T_0 is the initial temperature, Φ is the heating rate, and t is the time elapsed since the onset of heating. If inclusion and gas form a closed system, the evaporation flux must be balanced by a change in the vapor pressure $dP_{\ell,i}$ (we use the ideal gas law here),

$$\sum_\ell \frac{4\pi\mathcal{R}^3 dP_{\ell,i}}{3RT} = \sum_\ell \frac{\gamma_{\ell,i}\left(P_{eq,\ell,i}-P_{\ell,i}\right)}{\sqrt{2\pi m_{\ell,i}RT}} 4\pi r^2 dt. \quad \text{(S21)}$$

Different gas species can be lost at different rates depending on their masses and evaporation coefficients, so the speciation of the vaporized gas does not necessarily reflect equilibrium vapor pressures. We assume that once in the gas, the different gas species have the opportunity to re-equilibrate and we have,

$$P_{\ell,i} = \frac{P_{eq,\ell,i}}{P_{eq,i}} P_i. \quad \text{(S22)}$$

with $P_i = \sum_\ell P_{\ell,i}$ and $P_{eq,i} = \sum_\ell P_{eq,\ell,i}$. Using Eqs. S21 and S16-S18 ($P_{eq,\ell,i} = x_{\ell,i}P_{eq,i}$), we can rewrite Eq. S21 as,

$$\frac{dP_i}{dt} = 3\Upsilon_i\left(P_{eq,i} - P_i\right)\sqrt{\frac{RT}{2\pi}}\frac{r^2}{\mathcal{R}^3}, \quad \text{(S23)}$$

with $\Upsilon_i = \sum_\ell \gamma_{\ell,i} x_{\ell,i}/\sqrt{m_{\ell,i}}$. P_i is related to the total number of moles of i in the gas $\eta_{g,i}$ by the ideal gas law, and $P_{eq,i}$ is related to the total number of moles of i in the solid $\eta_{s,i}$ through Eq. S19. We thus have,

$$\frac{d\eta_{g,i}}{dt} = 3\Upsilon_i\left(\kappa_i \frac{4\pi\mathcal{R}^3\eta_{s,i}}{3RT\eta_{s,Ca}} - \eta_{g,i}\right)\sqrt{\frac{RT}{2\pi}}\frac{r^2}{\mathcal{R}^3}, \quad \text{(S24)}$$

where $\eta_{s,Ca}$ are the total number of Ca substitution sites in the solid. We consider that before vapor dissipation, gas and solid form a closed system, so we have $\eta_{g,i} + \eta_{s,i} = \eta_{tot,i}$ with $\eta_{tot,i}$ a constant. If we introduce $f_{g,i} = \eta_{g,i}/\eta_{tot,i}$ the fraction of i that has been evaporated, we have,

$$\frac{df_{g,i}}{dt} = 3\Upsilon_i\left[\kappa_i \frac{4\pi\mathcal{R}^3\,(1-f_{g,i})}{3RT\eta_{s,Ca}} - f_{g,i}\right]\sqrt{\frac{RT}{2\pi}}\frac{r^2}{\mathcal{R}^3}. \quad \text{(S25)}$$

If we assume that the precursor is made of hibonite, one can calculate the number of moles of Ca sites using the density ρ_{hib} and molar mass m_{hib} of hibonite,

$$\eta_{s,Ca} = \rho_{hib}\frac{4}{3}\pi r^3/m_{hib}. \quad \text{(S26)}$$

We therefore have for Eq. S25,

$$\frac{df_{g,i}}{dt} = \Upsilon_i\left[\frac{3m_{hib}\kappa_i}{\sqrt{2\pi RT}\rho_{hib}r}(1-f_{g,i}) - 3\sqrt{\frac{RT}{2\pi}}\frac{r^2}{\mathcal{R}^3}f_{g,i}\right]. \quad \text{(S27)}$$

If we change the differentiation variable from t to T and write $T = T(t)$, Eq. S27 becomes,

$$\frac{df_{g,i}}{dT} = \frac{\Upsilon_i}{\dot{T}}\left[\frac{3m_{hib}\kappa_i}{\sqrt{2\pi RT}\rho_{hib}r}(1-f_{g,i}) - 3\sqrt{\frac{RT}{2\pi}}\frac{r^2}{\mathcal{R}^3}f_{g,i}\right]. \quad \text{(S28)}$$

Assuming that the temperature increasing linearly with time, $T(t) = T_0 + \Phi t$, $\dot{T} = \Phi$. Equation S28 takes the form,

$$\frac{df_{g,i}}{dT} = \frac{\Upsilon_i}{\Phi}\left[\frac{3m_{hib}\kappa_i}{\sqrt{2\pi RT}\rho_{hib}r}(1 - f_{g,i}) - 3\sqrt{\frac{RT}{2\pi}}\frac{r^2}{\mathcal{R}^3}f_{g,i}\right]. \quad \text{(S29)}$$

Equation S29 can be integrated starting at a low temperature with the initial condition $f_{g,i} = 0\ at\ T = T_0$, and we get the fraction of element i evaporated,

$$f_{g,i} = e^{-\int_1^T \frac{\Upsilon_i}{\Phi}\left(\frac{3m_{hib}\kappa_i}{\sqrt{2\pi RT}\rho_{hib}r} + 3\sqrt{\frac{RT}{2\pi\mathcal{R}^3}}r^2\right)dT} \int_{T_0}^{T} \frac{\Upsilon_i}{\Phi}\frac{3m_{hib}\kappa_i}{\sqrt{2\pi RT}\rho_{hib}r} e^{\int_1^T \frac{\Upsilon_i}{\Phi}\left(\frac{3m_{hib}\kappa_i}{\sqrt{2\pi RT}\rho_{hib}r} + 3\sqrt{\frac{RT}{2\pi\mathcal{R}^3}}r^2\right)dT} dT. \quad \text{(S30)}$$

The isotopic composition was calculated by applying Eq. S30 to different isotopes of the REEs using $\delta_{g,i,2/1} = 1000\ln(f_{g,i,2}/f_{g,i,1})/(m_{i,2} - m_{i,1})$, where $m_{i,1}$ and $m_{i,2}$ are the molecular mass of isotope 1 and 2 of REE i respectively. The parameters that can differ in Eq. S29 between two isotopes are Υ_i and κ_i, where Υ_i is a function of $\gamma_{\ell,i}$, $x_{\ell,i}$ and $m_{\ell,i}$. We only vary $m_{\ell,i}$ and keep the other parameters constant. The fraction and the isotopic fractionation of the element evaporated are both functions of the heating rate and final temperature (duration) of the evaporation episode. We can therefore constrain the heating rate and duration from the depletion of the element considered relative to Sm (fraction evaporated), and the isotopic composition of the CAIs with group II REE patterns (corresponding to the composition of the gas except for Eu and Yb).

For numerical calculations, the precursor is assumed to be a sphere with radius *r* of 40 μm, a typical size for hibonite inclusions in Murchison (70 to 150 μm in their longest dimensions; (*58*)). The ambient pressure during evaporation is set to 10^{-3} bar H_2. We assume that the system has solar bulk composition. To calculate the whole system radius, we use $\aleph_{Ca}$ the number of moles of Ca condensed per unit volume of the system solid+gas, which is from an Excel spreadsheet provided as supplementary online material in (*15*). Indeed, we have $\aleph_{Ca}4\pi\mathcal{R}^3/3 = n_{Ca}4\pi r^3/3$ and $\mathcal{R} = r(n_{Ca}/\aleph_{Ca})^{1/3}$ where $n_{Ca} = 5.42$ mol/L is the Ca molar density of hibonite. The density ρ_{hib} and molar mass m_{hib} of the host mineral hibonite are 3.84 g/cm^3 and 708.8 g/mol, respectively. The radius of the system inclusion+gas $\mathcal{R}$ used is accordingly ~5 m. The sticking coefficients $\gamma_{\ell,i}$ of the REEs are not known and set to 0.1 based on the range of the sticking coefficients of Mg and SiO in melt of CAI composition (*9*). The oxygen fugacity P_O is from a previous condensation calculation (*3*) and is provided in an Excel spreadsheet in the Supplementary Online materials of (*15*). The molar masses $m_{M,i}$ of REEs used for calculation in g/mol are 138.91 (La), 140.12 (Ce), 140.91 (Pr), 144.24 (Nd), 150.36 (Sm), 151.96 (Eu), 157.25 (Gd), 158.93 (Tb), 162.50 (Dy), 164.93 (Ho), 167.26 (Er), 168.93 (Tm), 173.04 (Yb), 174.97 (Lu), respectively. Other thermodynamic data for the REEs, such as the Gibbs free energy and activity coefficients ($\chi_{\ell,i}$) can be found in the supplementary material of (*15*). The choice of the precursor size and thermodynamic data have little effect on the interpretation of the thermal event given the great difference in terms of timescales for the astrophysical events that are considered.

3. REE Abundance and Stable Isotopic Fractionation during Condensation

We envision a two-step process for establishing group II REE pattern. In the first step, all REEs except the most refractory ones are quantitatively evaporated (Sect. 2). This means that Eu and Yb are in the vapor. In the second step, the vapor thus produced is partially

condensed. Moderately refractory REEs are uniformly enriched in CAIs and display subdued stable isotopic fractionations. We therefore expect that during this condensation step, only the least refractory Eu and Yb remain in the vapor, while other REEs are quantitatively condensed.

Eu and Yb are depleted in CAIs with group II REE patterns but show rather subdued isotopic fractionations. This observation can be explained if condensation occurred under near-equilibrium conditions. Cooling must have been protracted to prevent the buildup of large supersaturation, thereby limiting the extent of kinetic isotopic fractionation. Indeed, if cooling had been fast, the equilibrium vapor pressure would have decreased rapidly and the rate of condensation of gas atoms would not have been sufficient to keep up with this decrease. Large kinetic isotope effects associated with supersaturation would have developed, which is not seen for Eu and Yb. Below, we present a model to translate our measurements into a quantitative assessment of cooling rates and timescales. We model condensation assuming closed-system behavior (also see (*22, 26*)) until gas dissipation.

We assume that the CAIs are of equal sizes and evenly distributed in space. We assume that during cooling and condensation, gas and CAI form a closed system. Elements condense following linear cooling until a time/temperature when vapor is dissipated. If the CAIs are all identical and evenly distributed, we do not need to track a whole ensemble of CAIs and can instead only consider a single CAI of radius r surrounded by a parcel of gas of finite volume $V_g = 4\pi\mathcal{R}^3/3$ with no-flux boundary conditions at the boundaries, which from a practical point of view is equivalent to considering a local closed-system. The decrease in the amount of element i in the gas residue is related to the condensation net flux,

$$-\sum_\ell \frac{4\pi\mathcal{R}^3 dP_{\ell,i}}{3RT} = \sum_\ell \frac{\gamma_{\ell,i}\left(P_{\ell,i}-P_{eq,\ell,i}\right)}{\sqrt{2\pi m_{\ell,i}RT}} 4\pi r^2 dt. \quad \text{(S31)}$$

The steps in the derivation of the differential equation governing condensation are similar to those used to derive Eq. S27 and will not be repeated here,

$$\frac{df_{s,i}}{dt} = \Upsilon_i \left[3\sqrt{\frac{RT}{2\pi}}\frac{r^2}{\mathcal{R}^3}\left(1-f_{s,i}\right) - \frac{3m_{hib}\kappa_i}{\sqrt{2\pi RT}\rho_{hib}r} f_{s,i}\right]. \quad \text{(S32)}$$

Changing the differentiation variable from t to T, and writing $T = T(t)$, we have,

$$\frac{df_{s,i}}{dT} = \frac{\Upsilon_i}{\dot{T}} \left[3\sqrt{\frac{RT}{2\pi}}\frac{r^2}{\mathcal{R}^3}\left(1-f_{s,i}\right) - \frac{3m_{hib}\kappa_i}{\sqrt{2\pi RT}\rho_{hib}r} f_{s,i}\right]. \quad \text{(S33)}$$

If we parameterize cooling as $T(t) = T_0 + \Phi t$, like in the evaporation section, with T_0 the starting temperature and Φ (a negative number) the cooling rate, we can write an equation similar to Eq. S29 for the solid condensate,

$$\frac{df_{s,i}}{dT} = \frac{\Upsilon_i}{\Phi} \left[3\sqrt{\frac{RT}{2\pi}}\frac{r^2}{\mathcal{R}^3}\left(1-f_{s,i}\right) - \frac{3m_{hib}\kappa_i}{\sqrt{2\pi RT}\rho_{hib}r} f_{s,i}\right]. \quad \text{(S34)}$$

Integrating Eq. S29 or S34 starting at a high temperature with the initial condition $f_{s,i} = 0 \; at \; T = T_0$, we can calculate the fraction of i that has condensed as a function of temperature,

$$f_{s,i} = e^{-\int_1^T \frac{\Upsilon_i}{\Phi}\left(\frac{3m_{hib}\kappa_i}{\sqrt{2\pi RT}\rho_{hib}r}+3\sqrt{\frac{RT}{2\pi\mathcal{R}^3}}r^2\right)dT} \int_{T_0}^{T} 3\frac{\Upsilon_i}{\Phi}\sqrt{\frac{RT}{2\pi}}\frac{r^2}{\mathcal{R}^3} e^{\int_1^T \frac{\Upsilon_i}{\Phi}\left(\frac{3m_{hib}\kappa_i}{\sqrt{2\pi RT}\rho_{hib}r}+3\sqrt{\frac{RT}{2\pi\mathcal{R}^3}}r^2\right)dT} dT. \quad \text{(S35)}$$

The numerical values used in the condensation calculation are very similar to those used during evaporation. The free parameters are the heating rate and duration of the evaporation, which can be constrained by combining measurements of the depletion and isotopic fractionation of Eu and Yb. In our calculation, we assume a starting temperature of 1700 K, at which hibonite is thought to have started condensing but REEs are still mostly in the gas phase.

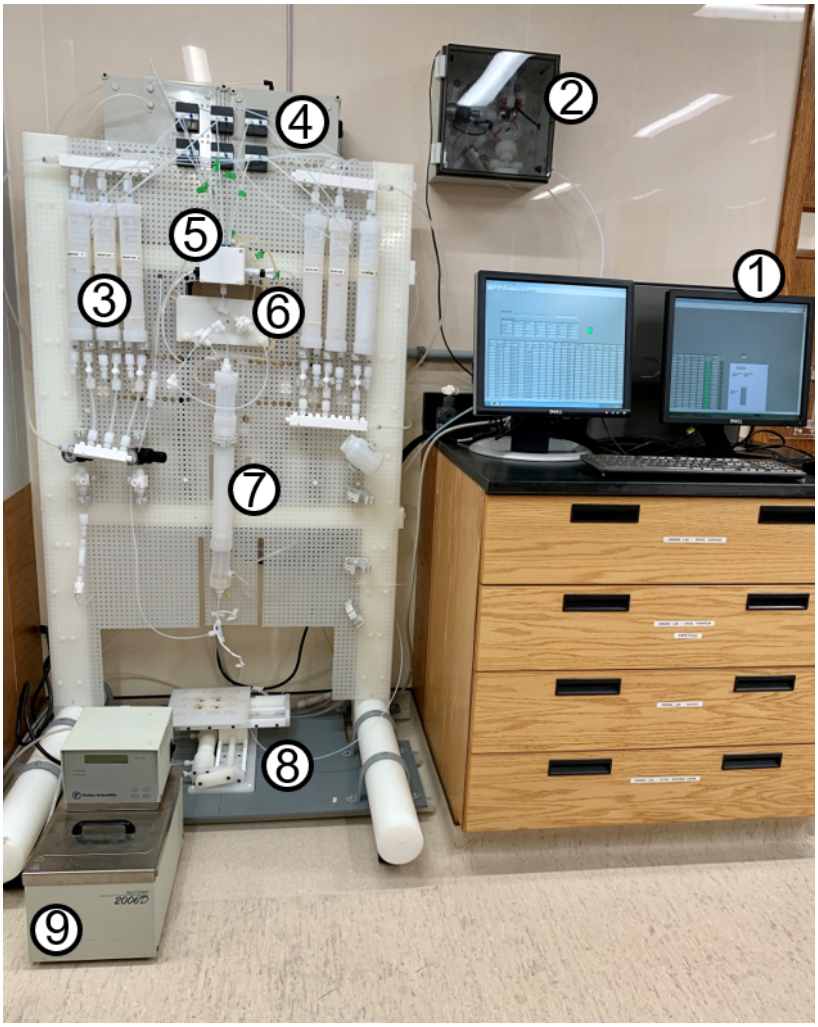

Fig. S1. FPLC system. 1. Control station with Labview software. **2.** Gas switch. If the pressure of the building-supplied high-purity N_2 from a nitrogen generator goes below 60 PSI, the gas source switches to a cylinder of compressed N_2. **3.** Temperature-controlled water/reagent reservoirs. **4.** Electronic bay and pneumatic PTFE positive displacement diaphragm metering pumps. The electronics are within a positively pressurized box to avoid contact with acid fumes. **5.** Temperature-controlled mixing chamber. Reagents introduced by the metering pumps are mixed using a magnetic stirring bar controlled by an external pneumatic micromotor. **6.** Sample introduction loop. **7.** Chromatography column. The column is made of a fine PTFE tube (1.6 mm inner diameter and 70 cm length here) that runs through a Teflon jacket where water is flowing at a set temperature. **8.** Stage. A 16-position pneumatic all-plastic stage is used to dispense the elution cuts in different beakers. **9.** Heating circulating water bath. Many modifications were made after (*29*), notably the conversion to all-pneumatic actuation (including fluoropolymer metering pumps), addition of a sample introduction loop, migration of the electronics to a positively-pressurized box, and development and implementation of a pneumatically-actuated plastic-made 16-position stage (*30*). Photo credit: Justin Hu, The University of Chicago.

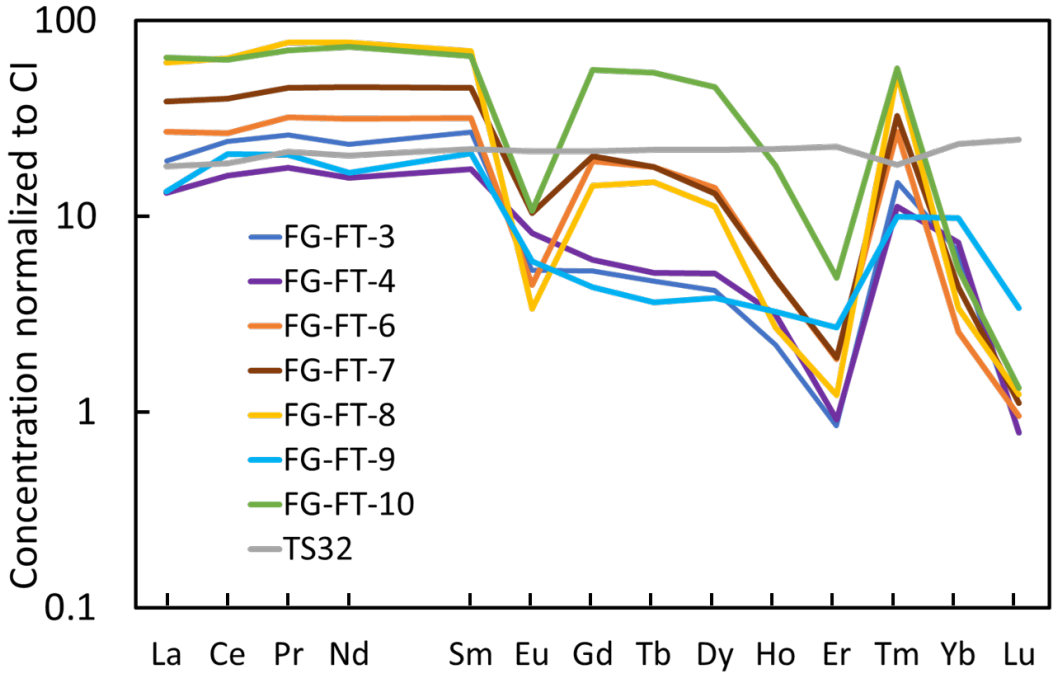

Fig. S2. REE abundance patterns of the 8 CAIs (7 with group II REE patterns) studied here, in order of atomic number (*15, 34*)**.**

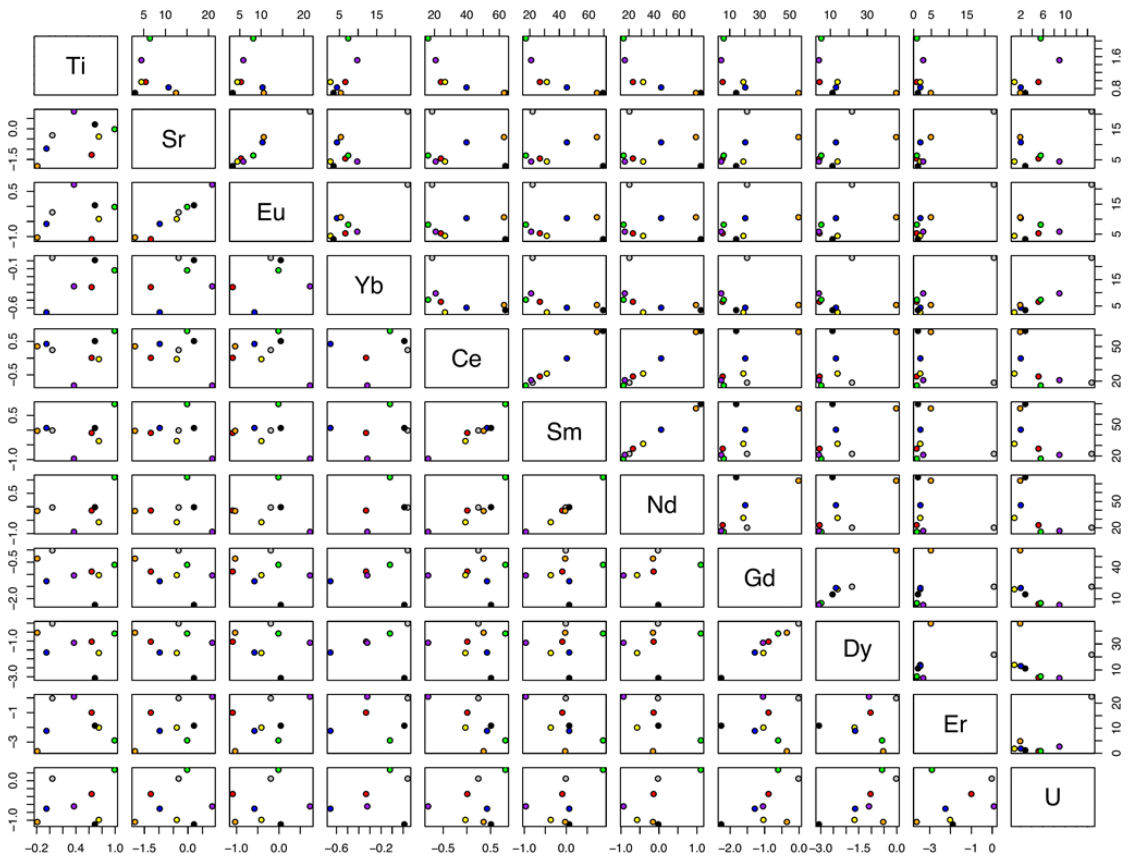

Fig. S3. Scatter plot matrix of 7 group II CAIs. The top right plots are correlations of the abundances normalized to CI chondrites, while the bottom left plots are the correlations of the stable isotopic fractionations (‰/amu). Circles in grey, red, green, yellow, blue, black, purple and orange correspond to CAIs TS32, FG-FT-3, 4, 6, 7, 8, 9 and 10, respectively. Note that in this diagram, none of the plots displays enrichment factor *vs*. isotopic composition (or vice versa).

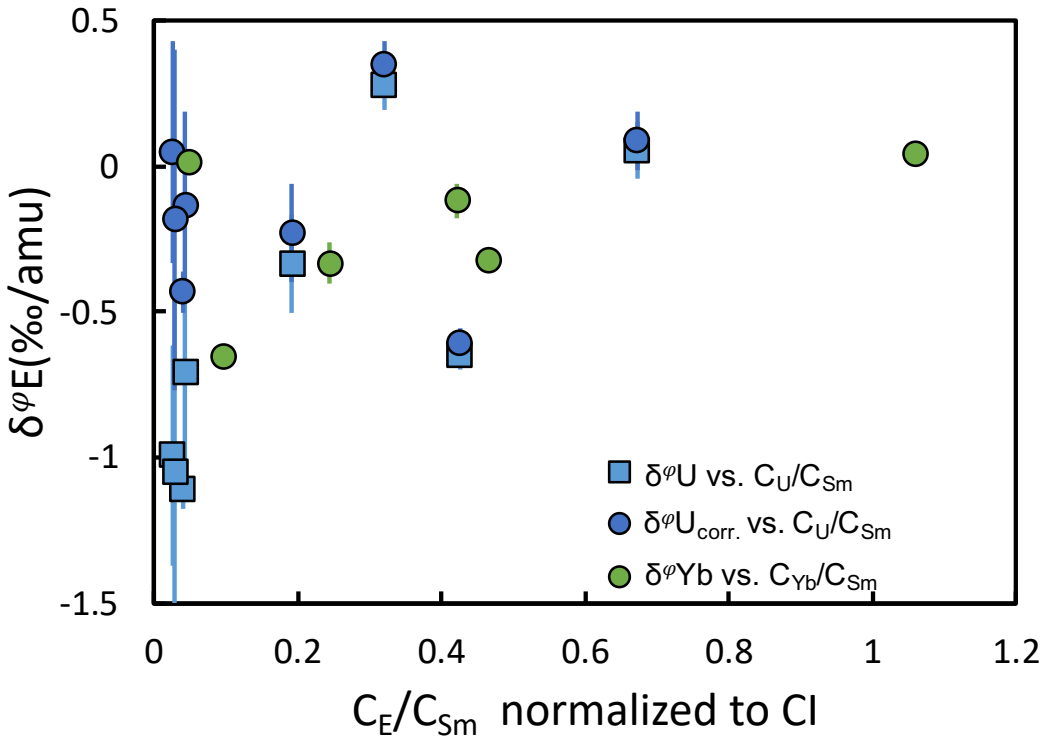

Fig. S4. Yb (green) and U (blue) isotopic compositions plotted as a function of their depletions relative to Sm in CAIs. The Yb isotopic data are from Table 1, while the U isotopic data are from (*34*). The blue-filled squares are raw U isotopic data (δ^{φ}U), while the blue filled-circles ($\delta^{\varphi}U_{corr.}$) have been corrected for decay of ^{247}Cm ($t_{1/2}$ = 15.6 My) using an initial $^{247}Cm/^{235}U$ ratio of 7.0×10^{-5} (*34, 59, 60*) and using the Nd/U ratio as a measure of the fractionation of the Cm/U ratio. As shown, the CAIs show no correlation between δ^{φ}Yb and δ^{φ}U, despite the broad logarithmic correlation of their concentrations (*34*). It is worth noting that the correlation in (*34*) is visible in logarithmic scale but the scatter in the data points around the 1:1 line spans an order of magnitude. The lack of correlation between δ^{φ}Yb and δ^{φ}U could be due to their distinct volatilities or due to U mobilization during aqueous alteration of fine-grained CAIs (*34*).

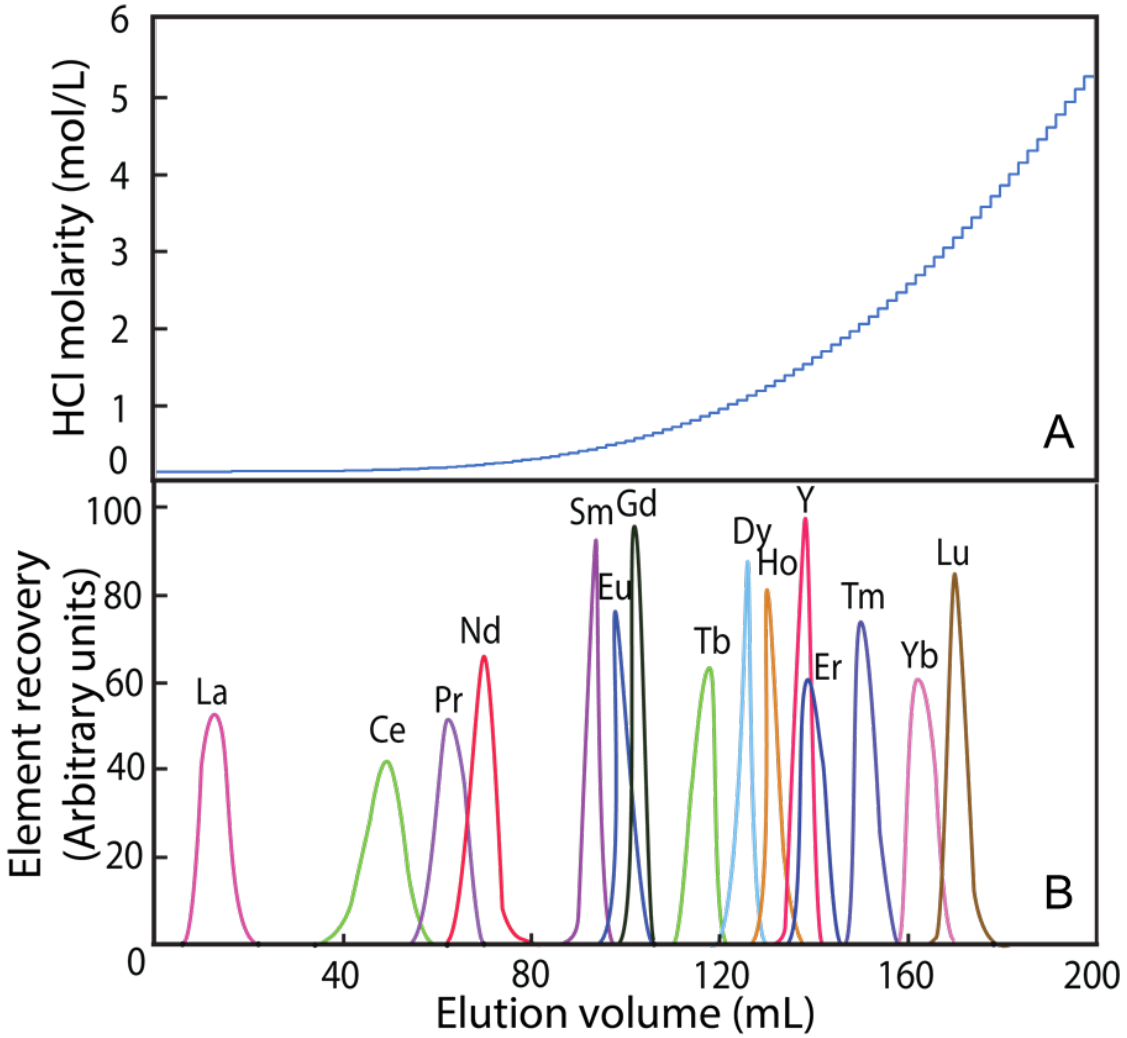

Fig. S5. FPLC elution curve of the REEs (**A**) HCl molarity of the elution solution injected in the column as a function of volume. (**B**) REE recovery as a function of elution volume. The chromatography column is 70 cm long, 1.6 mm in diameter, filled with 1.4 mL of Ln-Spec resin (*29*), and heated at 70 °C.

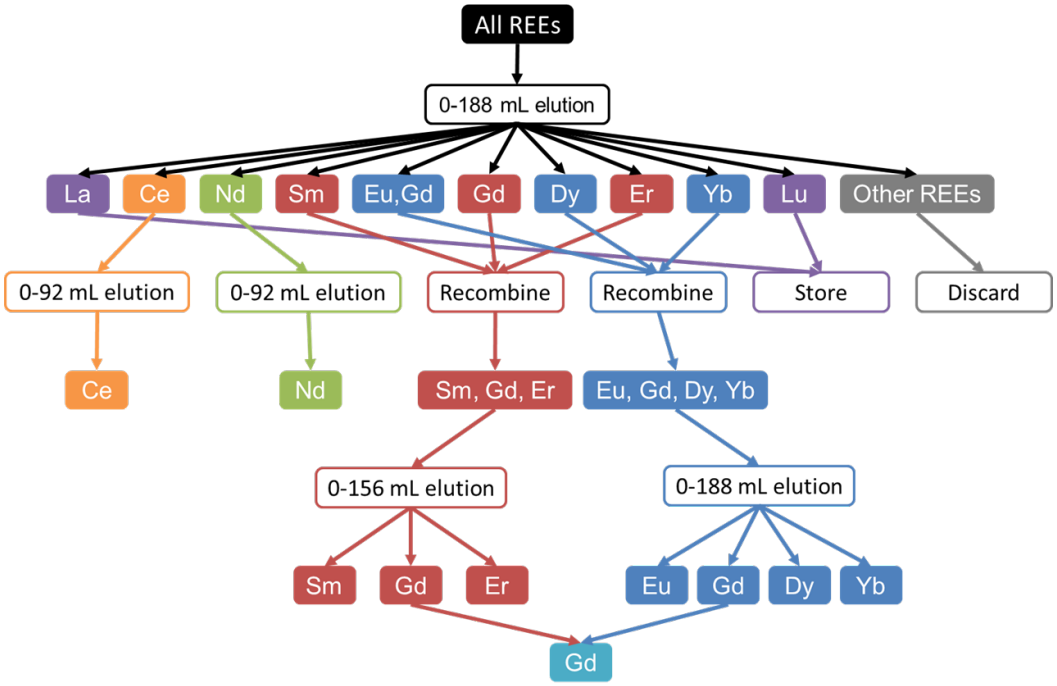

Fig. S6. Flowchart of 2-step FPLC elution of the REEs. Each elution in the flowchart uses the same gradient elution of HCl displayed in Fig. S5A but ends at different acid volume. After the first elution, REEs that are not neighbor to each other (*i.e.*, Sm/Gd/Er and Eu/Dy/Yb) are recombined and loaded onto the FPLC system (Fig. S1) for a second elution. The Eu cut from the first 0–188 mL elution contains minor Gd, which is separated from the second 0–188 mL elution and recombined with Gd cut from the 0–156 mL elution.

Table. S1. Titanium isotopic fractionation (determined by double spike) and isotopic anomalies of geostandards and CAIs

Sample	Name	ε^{46}Ti	ε^{48}Ti	ε^{50}Ti	δ^{Φ}Ti (SSB)	δ^{Φ}Ti (DS)
G3						0.21 ± 0.06
BCR2					0.01 ± 0.08	-0.01 ± 0.06
TS32		1.79 ± 0.06	0.45 ± 0.04	9.27 ± 0.09	0.07 ± 0.08	0.04 ± 0.06
ME-3364-22.2	FG-FT-2	1.61 ± 0.50	0.31 ± 0.30	9.76 ± 0.67	0.06 ± 0.12	0.30 ± 0.06
ME-3364-25.2	FG-FT-3	1.76 ± 0.36	0.48 ± 0.23	10.01 ± 0.32	0.24 ± 0.04	0.64 ± 0.06
ME-2639-16.2	FG-FT-4	1.77 ± 0.12	0.42 ± 0.07	9.35 ± 0.13	1.02 ± 0.07	0.99 ± 0.06
ME-2639-49.7	FG-FT-6	2.51 ± 0.55	-0.03 ± 0.40	12.98 ± 0.42	0.57 ± 0.52	0.75 ± 0.06
ME-2639-51.1	FG-FT-7	1.55 ± 0.57	0.25 ± 0.08	6.54 ± 0.30	-0.37 ± 0.19	-0.05 ± 0.06
AL3S5	FG-FT-8	1.52 ± 0.48	-0.46 ± 0.39	8.16 ± 0.88	0.32 ± 0.28	0.69 ± 0.06
AL4S6	FG-FT-9	2.02 ± 0.09	0.12 ± 0.05	13.71 ± 0.07	0.20 ± 0.05	0.36 ± 0.06
AL8S2	FG-FT-10	2.15 ± 1.98	0.53 ± 1.05	9.54 ± 1.53	-0.36 ± 0.57	-0.19 ± 0.06
AL10S1	FG-FT-11	1.97 ± 1.98	0.64 ± 1.05	9.39 ± 1.53	-0.63 ± 0.57	-0.20 ± 0.06

εTi is normalized to $^{49}Ti/^{47}Ti = 0.74977$; isotopic anomalies and stable isotopic fractionations (relative to the OL-Ti standard) using sample-standard bracketing (SSB) are published in (*15*). Some sample names in Table 1 of (*15*) were incorrect and are corrected in the present table.

Table. S2. Cup configuration of analyzed REEs.

		Cup configurations								
		L4	L3	L2	L1	C	H1	H2	H3	H4
Ce	Main	^{131}Xe	-	^{136}Ce	^{137}Ba	^{138}Ce	^{139}La	^{140}Ce	^{142}Ce	^{145}Nd
Nd	Main	^{140}Ce	^{142}Nd	^{143}Nd	^{144}Nd	^{145}Nd	^{146}Nd	^{148}Nd	^{150}Nd	^{152}Sm
Sm	Main	^{144}Sm	^{145}Nd*	^{147}Sm	^{148}Sm	^{149}Sm	^{150}Sm	^{152}Sm	^{154}Sm	^{156}Gd*
Eu	Main	-	^{151}Eu	^{153}Eu	^{156}Dy	^{158}Dy	^{161}Dy	^{162}Dy	^{164}Dy	^{166}Er*
Gd	Main	^{150}Sm*	^{152}Gd	^{154}Gd	^{155}Gd	^{156}Gd	^{157}Gd	^{158}Gd	^{160}Gd	^{162}Dy*
Dy	Main	^{156}Dy*	^{157}Gd*	^{158}Dy	^{160}Dy	^{161}Dy	^{162}Dy	^{163}Dy	^{164}Dy	-
	Sub	-	-	-	-	^{163}Dy^{n}	^{164}Dy	-	^{166}Er	-
Yb	Main	^{168}Yb	^{170}Yb	^{171}Yb	^{172}Yb	^{173}Yb	^{174}Yb	^{175}Lu*	^{176}Yb	^{180}Hf*
	Sub	^{166}Er	-	^{169}Tm	-	^{171}Yb	^{172}Yb	^{173}Yb^{n}	-	^{178}Hf

Faraday cups with * are connected to 10^{12} Ω amplifiers while the ones unlabeled are connected to 10^{11} Ω amplifiers.

Faraday cups with n are used to normalize the signals of subconfigurations to the main configurations.

REFERENCES AND NOTES

1. A. G. W. Cameron, The formation of the sun and planets. *Icarus* **1**, 13–69 (1962).
2. L. Grossman, Condensation in the primitive solar nebula. *Geochim. Cosmochim. Acta* **36**, 597–619 (1972).
3. S. Yoneda, L. Grossman, Condensation of CaO-MgO-Al_2O_3-SiO_2 liquids from cosmic gases. *Geochim. Cosmochim. Acta* **59**, 3413–3444 (1995).
4. T. Tanaka, A. Masuda, Rare-earth elements in matrix, inclusions, and chondrules of the Allende meteorite. *Icarus* **19**, 523–530 (1973).
5. B. Mason, S. R. Taylor, Inclusions in the Allende meteorite. *Smithson. Contrib. Earth Sci.* (1982).
6. T. R. Ireland, B. Fegley Jr., The solar system's earliest chemistry: Systematics of refractory inclusions. *Int. Geol. Rev.* **42**, 865–894 (2000).
7. N. Dauphas, A. Pourmand, Thulium anomalies and rare earth element patterns in meteorites and Earth: Nebular fractionation and the nugget effect. *Geochim. Cosmochim. Acta* **163**, 234–261 (2015).
8. J.-A. Barrat, N. Dauphas, P. Gillet, C. Bollinger, J. Etoubleau, A. Bischoff, A. Yamaguchi, Evidence from Tm anomalies for non-CI refractory lithophile element proportions in terrestrial planets and achondrites. *Geochim. Cosmochim. Acta* **176**, 1–17 (2016).
9. F. M. Richter, A. M. Davis, D. S. Ebel, A. Hashimoto, Elemental and isotopic fractionation of Type B calcium-, aluminum-rich inclusions: Experiments, theoretical considerations, and constraints on their thermal evolution. *Geochim. Cosmochim. Acta* **66**, 521–540 (2002).
10. A. Shahar, E. D. Young, Astrophysics of CAI formation as revealed by silicon isotope LA-MC-ICPMS of an igneous CAI. *Earth Planet. Sci. Lett.* **257**, 497–510 (2007).
11. F. M. Richter, P. E. Janney, R. A. Mendybaev, A. M. Davis, M. Wadhwa, Elemental and isotopic fractionation of type B CAI-like liquids by evaporation. *Geochim. Cosmochim. Acta* **71**, 5544–5564 (2007).
12. L. Grossman, S. B. Simon, V. K. Rai, M. H. Thiemens, I. D. Hutcheon, R. W. Williams, A. Galy, T. Ding, A. V. Fedkin, R. N. Clayton, T. K. Mayeda, Primordial compositions of refractory inclusions. *Geochim. Cosmochim. Acta* **72**, 3001–3021 (2008).
13. A. N. Krot, E. R. Scott, M. E. Zolensky, Mineralogical and chemical modification of components in CV3 chondrites: Nebular or asteroidal processing? *Meteoritics* **30**, 748–775 (1995).

14. J. I. Simon, M. K. Jordan, M. J. Tappa, E. A. Schauble, I. E. Kohl, E. D. Young, Calcium and titanium isotope fractionation in refractory inclusions: Tracers of condensation and inheritance in the early solar protoplanetary disk. *Earth Planet. Sci. Lett.* **472**, 277–288 (2017).
15. A. M. Davis, J. Zhang, N. D. Greber, J. Hu, F. L. Tissot, N. Dauphas, Titanium isotopes and rare earth patterns in CAIs: Evidence for thermal processing and gas-dust decoupling in the protoplanetary disk. *Geochim. Cosmochim. Acta* **221**, 275–295 (2018).
16. B. L. A. Charlier, F. L. H. Tissot, N. Dauphas, C. J. N. Wilson, Nucleosynthetic, radiogenic and stable strontium isotopic variations in fine-and coarse-grained refractory inclusions from Allende. *Geochim. Cosmochim. Acta* **265**, 413–430 (2019).
17. K. Lodders, Solar system abundances and condensation temperatures of the elements. *Astrophys. J.* **591**, 1220 (2003).
18. W. V. Boynton, Fractionation in the solar nebula: Condensation of yttrium and the rare earth elements. *Geochim. Cosmochim. Acta* **39**, 569–584 (1975).
19. A. M. Davis, L. Grossman, Condensation and fractionation of rare earths in the solar nebula. *Geochim. Cosmochim. Acta* **43**, 1611–1632 (1979).
20. A. S. Kornacki, B. Fegley Jr., The abundance and relative volatility of refractory trace elements in Allende Ca, Al-rich inclusions: Implications for chemical and physical processes in the solar nebula. *Earth Planet. Sci. Lett.* **79**, 217–234 (1986).
21. G. Pound, J. Hirth, Condensation and evaporation, nucleation and growth kinetics. *Prog. Mater. Sci.* **11** (1963).
22. F. M. Richter, Timescales determining the degree of kinetic isotope fractionation by evaporation and condensation. *Geochim. Cosmochim. Acta* **68**, 4971–4992 (2004).
23. A. Tsuchiyama, S. Tachibana, T. Takahashi, Evaporation of forsterite in the primordial solar nebula; rates and accompanied isotopic fractionation. *Geochim. Cosmochim. Acta* **63**, 2451–2466 (1999).
24. K. Ozawa, H. Nagahara, Chemical and isotopic fractionations by evaporation and their cosmochemical implications. *Geochim. Cosmochim. Acta* **65**, 2171–2199 (2001).
25. N. Dauphas, F. Poitrasson, C. Burkhardt, H. Kobayashi, K. Kurosawa, Planetary and meteoritic Mg/Si and δ^{30}Si variations inherited from solar nebula chemistry. *Earth Planet. Sci. Lett.* **427**, 236–248 (2015).
26. B. Bourdon, C. Fitoussi, Isotope fractionation during condensation and evaporation during planet formation processes. *ACS Earth Space Chem.* **4**, 1408–1423 (2020).

27. A. V. Fedkin, L. Grossman, F. J. Ciesla, S. B. Simon, Mineralogical and isotopic constraints on chondrule formation from shock wave thermal histories. *Geochim. Cosmochim. Acta* **87**, 81–116 (2012).
28. J. Jouzel, L. Merlivat, Deuterium and oxygen 18 in precipitation: Modeling of the isotopic effects during snow formation. *J. Geophys. Res. Atmos.* **89**, 11749–11757 (1984).
29. T. J. Ireland, F. L. H. Tissot, R. Yokochi, N. Dauphas, Teflon-HPLC: A novel chromatographic system for application to isotope geochemistry and other industries. *Chem. Geol.* **357**, 203–214 (2013).
30. N. Dauphas, F. L. Tissot, R. Yokochi, T. J. Ireland, J. Hu, U.S. Patent 9,884,266 (2018).
31. J. Jiun-San Shen, T. Lee, 138La anomaly in the early solar system. *Astrophys. J. Lett.* **596**, L109 (2003).
32. A. Pourmand, N. Dauphas, T. J. Ireland, A novel extraction chromatography and MC-ICP-MS technique for rapid analysis of REE, Sc and Y: Revising CI-chondrite and Post-Archean Australian Shale (PAAS) abundances. *Chem. Geol.* **291**, 38–54 (2012).
33. E. Albalat, P. Telouk, F. Albarède, Er and Yb isotope fractionation in planetary materials. *Earth Planet. Sci. Lett.* **355**, 39–50 (2012).
34. F. L. H. Tissot, N. Dauphas, L. Grossman, Origin of uranium isotope variations in early solar nebula condensates. *Sci. Adv.* **2**, e1501400 (2016).
35. F. Moynier, A. Bouvier, J. Blichert-Toft, P. Telouk, D. Gasperini, F. Albarede, Europium isotopic variations in Allende CAIs and the nature of mass-dependent fractionation in the solar nebula. *Geochim. Cosmochim. Acta* **70**, 4287–4294 (2006).
36. S. B. Simon, L. Grossman, A. M. Davis, Fassaite composition trends during crystallization of Allende Type B refractory inclusion melts. *Geochim. Cosmochim. Acta* **55**, 2635–2655 (1991).
37. N. Dauphas, M. Y. Hu, E. M. Baker, J. Hu, F. L. H. Tissot, E. Ercan Alp, M. Roskosz, J. Zhao, W. Bi, J. Liu, J.-F. Lin, N. X. Nie, A. Heard, SciPhon: A data analysis software for nuclear resonant inelastic X-ray scattering with applications to Fe, Kr, Sn, Eu and Dy. *J. Synchrotron Radiat.* **25**, 1581–1599 (2018).
38. S. Gabelnick, G. Reedy, M. Chasanov, Infrared spectra and structure of some matrix-isolated lanthanide and actinide oxides. *J. Chem. Phys.* **60**, 1167–1171 (1974).
39. A. Stracke, H. Palme, M. Gellissen, C. Münker, T. Kleine, K. Birbaum, D. Günther, B. Bourdon, J. Zipfel, Refractory element fractionation in the Allende meteorite: Implications for solar nebula

condensation and the chondritic composition of planetary bodies. *Geochim. Cosmochim. Acta* **85**, 114–141 (2012).

40. G. J. MacPherson, A. M. Davis, Refractory inclusions in the prototypical CM chondrite, Mighei. *Geochim. Cosmochim. Acta* **58**, 5599–5625 (1994).
41. H. Palme, F. Wlotzka, K. Nagel, A. El Goresy, An ultra-refractory inclusion from the Ornans carbonaceous chondrite. *Earth Planet. Sci. Lett.* **61**, 1–12 (1982).
42. S. B. Simon, A. M. Davis, L. Grossman, A unique ultrarefractory inclusion from the Murchison meteorite. *Meteorit. Planet. Sci.* **31**, 106–115 (1996).
43. M. Audard, P. Abrahám, M. M. Dunham, J. D. Green, N. Grosso, K. Hamaguchi, J. H. Kastner, A. Kóspál, G. Lodato, M. M. Romanova, Episodic accretion in young stars. *Protostars Planets VI* **387** (2014).
44. G. Herbig, EX Lupi: History and spectroscopy. *Astron. J.* **133**, 2679 (2007).
45. L. Hartmann, S. J. Kenyon, The FU orionis phenomenon. *Annu. Rev. Astron. Astrophys.* **34**, 207–240 (1996).
46. A. P. Boss, C. M. D. Alexander, M. Podolak, Cosmochemical consequences of particle trajectories during FU Orionis outbursts by the early Sun. *Earth Planet. Sci. Lett*. **345**, 18–26 (2012).
47. A. P. Boss, C. M. D. Alexander, M. Podolak, Evolution of CAI-sized Particles during FU Orionis Outbursts. I. Particle Trajectories in Protoplanetary Disks with Beta Cooling. *The Astrophysical Journal* **901**, 81 (2020).
48. P. Ábrahám, A. Juhász, C. P. Dullemond, Á. Kóspál, R. van Boekel, J. Bouwman, T. Henning, A. Moór, L. Mosoni, A. Sicilia-Aguilar, N. Sipos, Episodic formation of cometary material in the outburst of a young Sun-like star. *Nature* **459**, 224–226 (2009).
49. K. D. McKeegan, J. Aléon, J. Bradley, D. Brownlee, H. Busemann, A. Butterworth, M. Chaussidon, S. Fallon, C. Floss, J. Gilmour, M. Gounelle, G. Graham, Y. Guan, P. R. Heck, P. Hoppe, I. D. Hutcheon, J. Huth, H. Ishii, M. Ito, S. B. Jacobsen, A. Kearsley, L. A. Leshin, M.-C. Liu, I. Lyon, K. Marhas, B. Marty, G. Matrajt, A. Meibom, S. Messenger, S. Mostefaoui, S. Mukhopadhyay, K. Nakamura-Messenger, L. Nittler, R. Palma, R. O. Pepin, D. A. Papanastassiou, F. Robert, D. Schlutter, C. J. Snead, F. J. Stadermann, R. Stroud, P. Tsou, A. Westphal, E. D. Young, K. Ziegler, L. Zimmermann, E. Zinner, Isotopic compositions of cometary matter returned by Stardust. *Science* **314**, 1724–1728 (2006).

50. C. M. Lisse, J. Van Cleve, A. C. Adams, M. F. A'Hearn, Y. R. Fernández, T. L. Farnham, L. Armus, C. J. Grillmair, J. Ingalls, M. J. S. Belton, O. Groussin, L. A. Mc Fadden, K. J. Meech, P. H. Schultz, B. C. Clark, L. M. Feaga, J. M. Sunshine, Spitzer spectral observations of the Deep Impact ejecta. *Science* **313**, 635–640 (2006).
51. D. Brownlee, P. Tsou, J. Aléon, C. M. O'D. Alexander, T. Araki, S. Bajt, G. A. Baratta, R. Bastien, P. Bland, P. Bleuet, J. Borg, J. P. Bradley, A. Brearley, F. Brenker, S. Brennan, J. C. Bridges, N. D. Browning, J. R. Brucato, E. Bullock, M. J. Burchell, H. Busemann, A. Butterworth, M. Chaussidon, A. Cheuvront, M. Chi, M. J. Cintala, B. C. Clark, S. J. Clemett, G. Cody, L. Colangeli, G. Cooper, P. Cordier, C. Daghlian, Z. Dai, L. D'Hendecourt, Z. Djouadi, G. Dominguez, T. Duxbury, J. P. Dworkin, D. S. Ebel, T. E. Economou, S. Fakra, S. A. J. Fairey, S. Fallon, G. Ferrini, T. Ferroir, H. Fleckenstein, C. Floss, G. Flynn, I. A. Franchi, M. Fries, Z. Gainsforth, J.-P. Gallien, M. Genge, M. K. Gilles, P. Gillet, J. Gilmour, D. P. Glavin, M. Gounelle, M. M. Grady, G. A. Graham, P. G. Grant, S. F. Green, F. Grossemy, L. Grossman, J. N. Grossman, Y. Guan, K. Hagiya, R. Harvey, P. Heck, G. F. Herzog, P. Hoppe, F. Hörz, J. Huth, I. D. Hutcheon, K. Ignatyev, H. Ishii, M. Ito, D. Jacob, C. Jacobsen, S. Jacobsen, S. Jones, D. Joswiak, A. Jurewicz, A. T. Kearsley, L. P. Keller, H. Khodja, A. L. D. Kilcoyne, J. Kissel, A. Krot, F. Langenhorst, A. Lanzirotti, L. Le, L. A. Leshin, J. Leitner, L. Lemelle, H. Leroux, M.-C. Liu, K. Luening, I. Lyon, G. M. Pherson, M. A. Marcus, K. Marhas, B. Marty, G. Matrajt, K. M. Keegan, A. Meibom, V. Mennella, K. Messenger, S. Messenger, T. Mikouchi, S. Mostefaoui, T. Nakamura, T. Nakano, M. Newville, L. R. Nittler, I. Ohnishi, K. Ohsumi, K. Okudaira, D. A. Papanastassiou, R. Palma, M. E. Palumbo, R. O. Pepin, D. Perkins, M. Perronnet, P. Pianetta, W. Rao, F. J. M. Rietmeijer, F. Robert, D. Rost, A. Rotundi, R. Ryan, S. A. Sandford, C. S. Schwandt, T. H. See, D. Schlutter, J. Sheffield-Parker, A. Simionovici, S. Simon, I. Sitnitsky, C. J. Snead, M. K. Spencer, F. J. Stadermann, A. Steele, T. Stephan, R. Stroud, J. Susini, S. R. Sutton, Y. Suzuki, M. Taheri, S. Taylor, N. Teslich, K. Tomeoka, N. Tomioka, A. Toppani, J. M. Trigo-Rodríguez, D. Troadec, A. Tsuchiyama, A. J. Tuzzolino, T. Tyliszczak, K. Uesugi, M. Velbel, J. Vellenga, E. Vicenzi, L. Vincze, J. Warren, I. Weber, M. Weisberg, A. J. Westphal, S. Wirick, D. Wooden, B. Wopenka, P. Wozniakiewicz, I. Wright, H. Yabuta, H. Yano, E. D. Young, R. N. Zare, T. Zega, K. Ziegler, L. Zimmerman, E. Zinner, M. Zolensky, Comet 81P/Wild 2 under a microscope. *Science* **314**, 1711–1716 (2006).
52. M. E. Zolensky, T. J. Zega, H. Yano, S. Wirick, A. J. Westphal, M. K. Weisberg, I. Weber, J. L. Warren, M. A. Velbel, A. Tsuchiyama, P. Tsou, A. Toppani, N. Tomioka, K. Tomeoka, N. Teslich,

M. Taheri, J. Susini, R. Stroud, T. Stephan, F. J. Stadermann, C. J. Snead, S. B. Simon, A. Simionovici, T. H. See, F. Robert, F. J. M. Rietmeijer, W. Rao, M. C. Perronnet, D. A. Papanastassiou, K. Okudaira, K. Ohsumi, I. Ohnishi, K. Nakamura-Messenger, T. Nakamura, S. Mostefaoui, T. Mikouchi, A. Meibom, G. Matrajt, M. A. Marcus, H. Leroux, L. Lemelle, L. Le, A. Lanzirotti, F. Langenhorst, A. N. Krot, L. P. Keller, A. T. Kearsley, D. Joswiak, D. Jacob, H. Ishii, R. Harvey, K. Hagiya, L. Grossman, J. N. Grossman, G. A. Graham, M. Gounelle, P. Gillet, M. J. Genge, G. Flynn, T. Ferroir, S. Fallon, D. S. Ebel, Z. R. Dai, P. Cordier, B. Clark, M. Chi, A. L. Butterworth, D. E. Brownlee, J. C. Bridges, S. Brennan, A. Brearley, J. P. Bradley, P. Bleuet, P. A. Bland, R. Bastien, Mineralogy and petrology of comet 81P/Wild 2 nucleus samples. *Science* **314**, 1735–1739 (2006).

53. S. Simon, A. Davis, L. Grossman, Origin of compact type A refractory inclusions from CV3 carbonaceous chondrites. *Geochim. Cosmochim. Acta* **63**, 1233–1248 (1999).
54. Q. R. Shollenberger, J. Render, G. A. Brennecka, Er, Yb, and Hf isotopic compositions of refractory inclusions: An integrated isotopic fingerprint of the solar system's earliest reservoir. *Earth Planet. Sci. Lett.* **495**, 12–23 (2018).
55. N. D. Greber, N. Dauphas, I. S. Puchtel, B. A. Hofmann, N. T. Arndt, Titanium stable isotopic variations in chondrites, achondrites and lunar rocks. *Geochim. Cosmochim. Acta* **213**, 534–552 (2017).
56. J. Y. Hu, N. Dauphas, Double-spike data reduction in the presence of isotopic anomalies. *J. Anal. At. Spectrom.* **32**, 2024–2033 (2017).
57. M.-A. Millet, N. Dauphas, Ultra-precise titanium stable isotope measurements by double-spike high resolution MC-ICP-MS. *J. Anal. At. Spectrom.* **29**, 1444–1458 (2014).
58. T. R. Ireland, Correlated morphological, chemical, and isotopic characteristics of hibonites from the Murchison carbonaceous chondrite. *Geochim. Cosmochim. Acta* **52**, 2827–2839 (1988).
59. G. A. Brennecka, S. Weyer, M. Wadhwa, P. E. Janney, J. Zipfel, A. D. Anbar, 238U/235U variations in meteorites: Extant 247Cm and implications for Pb-Pb dating. *Science* **327**, 449–451 (2010).
60. H. Tang, M.-C. Liu, K. D. McKeegan, F. L. Tissot, N. Dauphas, In situ isotopic studies of the U-depleted Allende CAI Curious Marie: Pre-accretionary alteration and the co-existence of 26Al and 36Cl in the early solar nebula. *Geochim. Cosmochim. Acta* **207**, 1–18 (2017).